Single-Molecule Fluorescence Studies of Membrane Transporters Using Total Internal Reflection Microscopy

Goudsmits, Joris M H; van Oijen, Antoine M; Slotboom, Dirk J

Published in:
Methods in Enzymology

DOI:
10.1016/bs.mie.2017.05.009

Publication date:
2017

CHAPTER FOUR

Single-Molecule Fluorescence Studies of Membrane Transporters Using Total Internal Reflection Microscopy

Joris M.H. Goudsmits, Antoine M. van Oijen[1,2], Dirk J. Slotboom[2]

University of Groningen, Groningen, The Netherlands
[2]Corresponding authors: e-mail address: vanoijen@uow.edu.au; d.j.slotboom@rug.nl

Contents

1. Introduction 102
2. Preparing Membrane Proteins and Lipid Membranes 105
   2.1 Protein Purification and Labeling 108
   2.2 Lipid Mixture Preparation 109
   2.3 Membrane Reconstitution 109
3. Single-Molecule Fluorescence Microscopy 110
   3.1 Glass Functionalization and Flow Cell Construction 111
   3.2 Experimental Setup and Image Acquisition 113
4. Data Analysis 115
   4.1 Subtraction of Electronic Offset 116
   4.2 Laser Profile Correction 116
   4.3 Dual View Alignment 116
   4.4 Drift Correction 117
   4.5 Data Analysis 117
Acknowledgments 118
References 118

Abstract

Cells are delineated by a lipid bilayer that physically separates the inside from the outer environment. Most polar, charged, or large molecules require proteins to reduce the energetic barrier for passage across the membrane and to achieve transport rates that are relevant for life. Here, we describe techniques to visualize the functioning of membrane transport proteins with fluorescent probes at the single-molecule level. First, we

[1] Present address: School of Chemistry, University of Wollongong, Wollongong, New South Wales, Australia.

Methods in Enzymology, Volume 594
ISSN 0076-6879
http://dx.doi.org/10.1016/bs.mie.2017.05.009

explain how to produce membrane-reconstituted transporters with fluorescent labels. Next, we detail the construction of a microfluidic flow cell to image immobilized proteoliposomes on a total internal reflection fluorescence microscope. We conclude by describing the methods that are needed to analyze fluorescence movies and obtain useful single-molecule data.

1. INTRODUCTION

Cells are the fundamental units of life, both structurally and functionally. The interior of a cell is enclosed by a membrane comprised of a lipid bilayer with a thickness of approximated 5 nm in which proteins are embedded. The membrane bilayer is a dynamic and fluid structure. Although the (protein-free) lipid bilayer is impermeable to macromolecules, some small and nonpolar molecules, such as O_2 and CO_2 can partition into the lipid bilayer, and thus diffuse across (Missner & Pohl, 2009). Uncharged polar molecules, such as H_2O and glycerol will also diffuse through, tough at (much) lower rates. Charged molecules, such as inorganic ions, are usually unable to pass the hydrophobic core of the bilayer because the energetic cost of dehydration is too high.

In order to precisely control intracellular solute concentrations and to allow transport of polar and charged molecules at useful rates, cells employ dedicated, membrane-integrated transport proteins. The high portion of genes encoding for transport proteins reflects their importance: 20%–30% of genes encodes for membrane proteins (Krogh, Larsson, von Heijne, & Sonnhammer, 2001), half of which are transporters (Ren & Paulsen, 2005). Transport proteins are divided in two main classes: passive and active transporters (Saier, Reddy, Tamang, & Vastermark, 2014). Passive transporters are catalysts that allow substrate molecules to flow in the direction of their chemical gradient across the membrane. Active transporters use different sources of energy to transport a specific molecule or class of molecules against a gradient. They can for example use ATP, the electrochemical gradient of a cosubstrate (for instance protons or Na^+), or light.

Extensive structural and biochemical investigations already have provided great understanding of membrane transporters (Drew & Boudker, 2016; Groeneveld & Slotboom, 2010). These techniques provide ensemble-averaged readouts and thereby conceal many aspects of the dynamics of individual members of the unsynchronized population.

Single-molecule techniques overcome this limit by directly probing individual proteins, allowing observation of short-lived intermediate states and rare events, and thereby providing new insights into important structural and functional properties. The first single-molecule observations were made in the 1970s by the detection of currents in single ion channels (Neher & Sakmann, 1976). Advances such as the detection of single fluorescent molecules under biologically relevant conditions (Brooks Shera, Seitzinger, Davis, Keller, & Soper, 1990) and single fluorescent proteins (Dickson, Cubitt, Tsien, & Moerner, 1997), as well as the continuous improvement of high-sensitivity and low-noise photon detectors have made single-molecule fluorescence techniques a powerful tool to study membrane proteins in vitro and in vivo (Akyuz, Altman, Blanchard, & Boudker, 2013; Erkens, Hanelt, Goudsmits, Slotboom, & van Oijen, 2013; Sako, Minoghchi, & Yanagida, 2000; Zhao et al., 2010). Other methods such as atomic force microscopy have been established as well to probe the dynamics of single membrane proteins and transporters (Ruan et al., 2017; Whited & Park, 2014), however fluorescence techniques allow for the parallel observation of many single transport proteins under dynamic environmental conditions. In this chapter, we focus on in vitro fluorescence techniques that we will describe in more detail later.

Fluorescence is the radiative decay, in the form of light, from a molecular singlet state back into the ground state from which the molecule has been excited (Lakowicz, 2006). The wavelength of the emitted light is typically higher than the wavelength of the light used for excitation; a phenomenon called Stokes shift. Fluorophores—or dyes—are specifically designed molecules with optimized fluorescence properties such as stability, brightness, and pH sensitivity (Gust et al., 2014). When chemically linked to a protein (or other molecule), their readouts provide information that can provide insight in the protein's structure and function in several ways, some of which will be described later (Weiss, 1999) (Fig. 1). First, they can be utilized in fluorescence microscopy to determine the spatial position with a potential accuracy of a few tens of nanometers. Although the point source of light produces a spot (point spread function—PSF) with a diameter that is fundamentally limited by the wavelength of the light, the center can be localized much more accurately (Schmidt, Schuetz, Baumgartner, Gruber, & Schindler, 1995) (Fig. 1A). When two host molecules are labeled with fluorophores with different spectral properties (i.e., different colors), their possible colocation can be studied. Second, intensity fluctuations of a single dye can

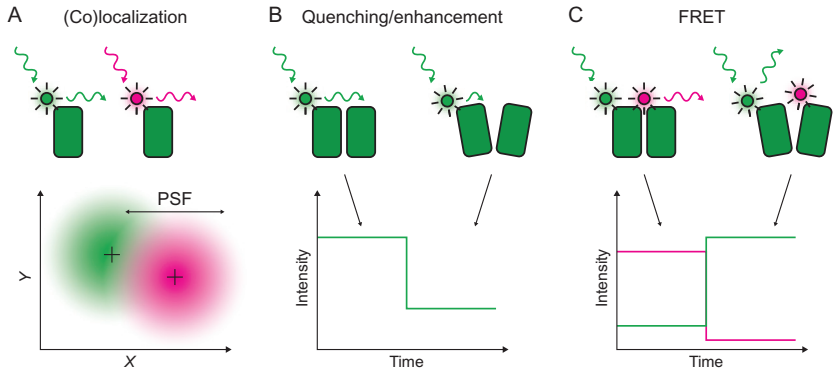

Fig. 1 Fluorescence detection techniques. Several fluorescence techniques; principle (*top*) and observable (*bottom*). (A) By fitting the PSF (typically a few 100 nm wide), the fluorophore can be localized (crosshairs) with an accuracy of a few 10 nm. Using multiple colors can hint for colocalization. (B) Changes in local environment, which can depend on protein conformation, of the fluorophore can cause quenching or enhancement. (C) FRET can be used to measure small distance changes between roughly 20 and 100 Å.

report on the activity or dynamics of proteins (Lu, Xun, & Xie, 1998) (Fig. 1B). A change in the local environment of the dye caused by protein function may quench or enhance fluorescence. Lastly, fluorescence (or Förster) resonance energy transfer (FRET) can provide information on protein dynamics and mechanistic insight in protein function. FRET is a mechanism based on the nonradiative transfer of excitation energy from a donor to an acceptor fluorophore (Ha et al., 1996). This transfer results in a decreased fluorescence intensity of the donor, and an increased intensity of the acceptor. The efficiency E of the transfer depends on the distance R between donor and acceptor:

$$E = \frac{1}{1 + (R/R_0)^6}.$$

Here R_0 is the Förster distance at which the efficiency is 50%. The Förster distance depends on the properties of the pair of dyes and is typically between 50 and 80 Å. The anticorrelated intensity changes of donor and acceptor dyes are the hallmark of FRET transients (Fig. 1C). When both dyes are positioned appropriately, it allows the detection of the interaction between molecules or structural changes within a biomolecule on the length scale of a few nanometers.

In this chapter, we focus on the single-molecule imaging of liposome-reconstituted membrane transport proteins using total internal reflection fluorescence (TIRF) microscopy. In the following sections, we will explain the relevant techniques and give a step-by-step description on how to setup, perform, and interpret single-molecule experiments.

2. PREPARING MEMBRANE PROTEINS AND LIPID MEMBRANES

Visualizing inter- and intraprotein dynamics requires the specific fluorescence labeling of subunits in the protein complex. We make use of the thiol-maleimide coupling reaction, which is highly specific at pH values below 7.5, to label cysteines in the folded state of the protein with the appropriate dye molecule, but other labeling chemistries can be used as long as they allow specific and efficient labeling. A cysteine mutant of the protein is designed to specifically position one or more labels in order to observe a change in fluorescence properties of the labels. Any native cysteine that is accessible to undesired maleimide labeling should be replaced by a suitable amino acid, for example serine. Remaining cysteines that cannot be removed without loss of function must be checked for undesirable labeling. Before labeling of engineered cysteines, DTT (dithiothreitol) or TCEP (*tris*-(2-carboxyethyl)phosphine) can be added as a reducing agent to break unwanted disulfide bonds that may have formed. However, excess of these agents must be removed by dialysis prior to adding the reactive dye molecule. Detergent-solubilized membrane proteins are labeled when attached to an affinity-tag column, which is used in the purification procedure. Subsequently, size-exclusion chromatography is performed, in order that remaining unreacted dye molecules are separated, and afterward the purified protein is reconstituted in a lipid bilayer (see later). Sometimes, a 100% labeling efficiency is required to visualize all components. However, occasionally only lower labeling efficiencies can be achieved. Also, homooligomeric proteins sometimes demand lower efficiencies: for example, a dimer might need only one fluorescent label, or a trimer exactly two (different) labels for FRET measurements. Optimizing dye concentrations and dye incubation times yields the desired average, but postacquisition single-molecule analysis (see later) will discern the stoichiometry.

Owing to its size and water solubility, a fluorescent label can alter the properties of the host protein. Therefore, it is crucial to assess the function of the labeled protein complex in detergent micelles or a lipid bilayer (see

later) with for example ATP and transport activity essays, which are outside of the scope of this chapter (Geertsma, Nik Mahmood, Schuurman-Wolters, & Poolman, 2008). Ideally, labeling should not affect the transport activity, but often leads to somewhat decreased activity. It is important to exclude that the remaining activity after labeling is not the result of the fraction of unlabeled protein. The fractional activity after labeling must therefore be higher than the fraction of unlabeled proteins.

Membrane proteins are naturally embedded in a lipid bilayer, providing a complex and dynamic environment. The proteins have to be removed from their native surroundings by detergent solubilization (Helenius & Simons, 1975), before they can be purified. Later, they can be analyzed further in the detergent solution, or, after reconstitution, in a (synthetic) lipid environment. Mimicking the complex and dynamic native environment is nontrivial. Biological membranes consist of multiple components that determine properties such as thickness, strength, and tension (Seddon, Curnow, & Booth, 2004). At the same time, membrane proteins interact with the surrounding lipids (Lee, 2003; Marsh, 2008), affecting protein folding and functioning (Lee, 2004; Phillips, Ursell, Wiggins, & Sens, 2009). Carefully choosing the lipids used for protein reconstitution minimizes any negative effects. Prokaryotic transporters are typically reconstituted in a synthetic mixture of dioleoyl-phosphatidylethanolamine (DOPE), dioleoyl-phosphatidylglycerol (DOPG), and dioleoyl-phosphatidylcholine (DOPC), as they often require a significant fraction of nonbilayer (i.e., cone shaped, as opposed to cylinder shaped) lipids (DOPE) and anionic lipids (DOPG) (Geertsma et al., 2008). For eukaryotic systems, typically a sterol is included as well.

A synthetic lipid bilayer reconstituted in vitro resembles the native environment much more closely than a detergent micelle—the latter may alter the protein's function as reflected by various studies (Akyuz et al., 2013; Dorwart, Wray, Brautigam, Jiang, & Blount, 2010; Erkens et al., 2013; Goudsmits, Slotboom, & van Oijen, 2017; Lewinson, Lee, Locher, & Rees, 2010; Mi et al., 2008). Membrane proteins can be reconstituted into nanodiscs (Ritchie et al., 2009) or liposomes (Rigaud & Levy, 2003) of various sizes (Fig. 2). Nanodiscs are small disc-shaped patches of membrane surrounded by scaffolding proteins acting as a belt; the diameter of around 10 nm can be controlled by the length of the scaffolding proteins that define the circumference of the disc (Fig. 2A). Embedded integral membrane proteins are experimentally accessible from both sides. Liposomes, in contrast,

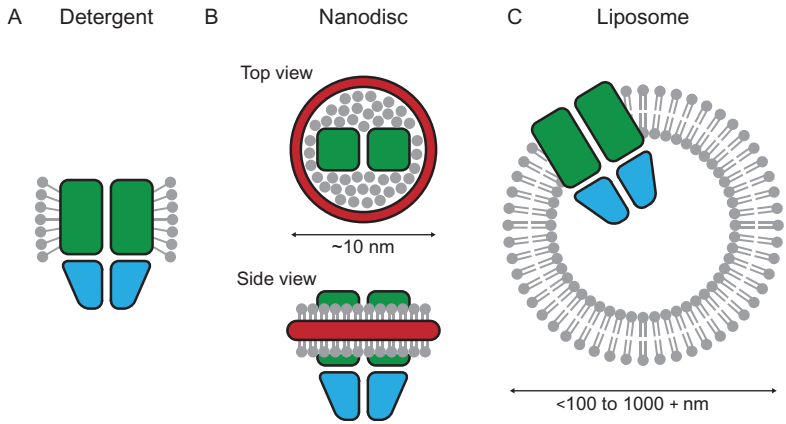

Fig. 2 Environment of membrane proteins. (A) In an aqueous environment, membrane proteins can be stabilized in detergent. Here the hydrophobic tails of the detergent molecules cover the protein and mimic the bilayer. Nanodiscs (B) and liposomes (C) resemble the native environment most closely. (B) In nanodiscs, a scaffolding protein (*red*) holds a patch of lipids together while the membrane protein is accessible from either side. (C) Liposomes on the other hand allow for gradients and allow only the outside to be accessible during the measurement, which is beneficial for studying transport.

have a luminal compartment that is not accessible to membrane-impermeable compounds, but it is possible to preload the inside with desired constituents during preparation of the liposomes (Fig. 2B). The diameters of liposomes vary from below 100 nm to tens of micrometers; unilaminar liposomes are typically in the lower size range. The compartmentalization offered by liposomes allows the establishment of membrane gradients, which makes them of great interest for studying transport. In this chapter, we focus on transport proteins reconstituted in 100-nm liposomes.

Protein reconstitution into liposomes involves mixing of the constituents—proteins and lipids—in the appropriate ratio, followed by detergent removal (for instance by adsorption to polystyrene beads). For single-molecule studies, the number of membrane complexes per liposome is a trade-off between high yield (not too many empty liposomes) and a low probability of multiple complexes per liposome. The optimal average value is around 0.1, resulting in—based on the Poisson distribution—roughly 10% of the liposomes with one complex, 0.5% of the liposomes (meaning 5% of the protein-containing liposomes) with more than one complex, and the remaining 90.5% being empty.

2.1 Protein Purification and Labeling

The following protocol is carried out at 4°C. We set out with membrane vesicles, thawed from a −80°C stock. For immobilization of the protein, we use an *octa*-histidine tag (His_8 tag) on the protein in combination with nickel affinity chromatography here, but any other suitable method can be substituted. Buffers used are 50 m*M* KPi, 200 m*M* KCl, pH 7.5 (buffer A), or the same buffer supplemented with 0.03% dodecyl maltoside (DDM, Anatrace) (buffer B).

1. Solubilize membrane vesicles in buffer A + 1% DDM; mix well and incubate for 1 h.
2. Centrifuge for 20 min at 80,000 rpm to separate insoluble material from detergent-solubilized proteins: decant supernatant in clean tube.
3. Add 500 μL (bed volume) of Ni Sepharose beads (GE Healthcare) washed in buffer B.
4. Incubate for 1 h while gently moving.
5. Add mixture to an empty disposable column and discard flow through.
6. Wash with 10 mL buffer B + 50 m*M* imidazole to remove nonspecifically bound proteins; discard flow through.
7. Label proteins with 0.5 mL dye solution (50 μg dye in 0.5 mL buffer B), incubate for 10–100 min (depending on desired labeling efficiency), mix well from time to time. In case a protein with two labeling sites has to be labeled with two different labels, typically a one-to-one molar ratio of dyes is used; the proper label stoichiometry is selected in postacquisition processing.
8. Wash with 10 mL buffer B to remove unreacted dye molecules; discard flow through.
9. Elute the protein with 2 mL buffer B + 500 m*M* imidazole and collect 500 μL fractions (four fractions in total). The second fraction contains the labeled protein.
10. Perform size-exclusion chromatography (Superdex-200 column, GE Healthcare) to further purify protein from aggregates and remaining free dye molecules, and directly use for reconstitution into liposomes (see later).

In case a soluble protein needs to by copurified (for example a soluble binding protein), the protein can be purified separately with the protocol as described earlier (starting from step 3 with cell extract, and with buffer A instead of buffer B) and mixed with the membrane protein before or after size-exclusion chromatography.

2.2 Lipid Mixture Preparation

Lipid mixtures are prepared separately and can be stored for up to several months in liquid nitrogen to prevent oxidation. They are prepared from the following lipids (dissolved in chloroform): 1,2-dioleoyl-sn-glycero-3-phosphocholine (DOPC); 1,2-dioleoyl-sn-glycero-3-phosphoethanolamine (DOPE); 1,2-dioleoyl-sn-glycero-3-phospho-(19-rac-glycerol) (DOPG); and 1,2-dioleoyl-sn-glycero-3-phosphoethanolamine-*N*-(cap biotinyl) (biotin-DOPE).

1. Mix (w/w) 40% DOPC, 30% DOPE, 30% DOPG, and 1% biotin-DOPE (used for surface immobilization, see later), in total 80 mg. The total amount can be scaled as desired.
2. Evaporate chloroform using rotary evaporation.
3. Add 4 mL buffer A (20 mg/mL) and incubate on ice for 30 min.
4. Dissolve lipids by shaking and aliquot in 400 μL (8 mg).
5. *Optional*: Lipids can be stained with lipophilic tracers (for example DiO, DiI, and DiD) in order to visualize liposomes in microscopy experiments. To this end, mix lipids with the appropriate marker in a 10,000:1 molar ratio, yielding approximately 9 dye molecules per 100-nm liposome (a 100-nm liposome contains roughly 9×10^4 lipid molecules).
6. Subject the mixture to four freeze–thaw cycles (frozen in liquid nitrogen and thawed at room temperate) to homogenize the lipid (and the tracer if applicable) distribution.

2.3 Membrane Reconstitution

A thawed lipid mixture aliquot (8 mg lipids in 400 μL) is used with fresh protein (at least 200 μL of 0.1 μ*M* membrane protein is required) to start a reconstitution. Soluble protein, if required on the inside of liposomes, is added in the appropriate concentration. The following steps are carried out at 4°C.

1. Extrude lipid mixture with 400-nm filter (Mini-Extruder with polycarbonate filter, Avanti Polar Lipids) to create unilamellar liposomes (note that 400 nm is not yet the final size of the liposomes). Extrude an uneven number of times; 11 times is sufficient.
2. Mix empty liposomes (10 mg/mL, final), membrane protein (0.02 μ*M*, final), soluble protein (if applicable; 3.2 μ*M* final equates to on average 1 molecule of soluble protein in a 100-nm liposome), and Triton X-100 (Sigma-Aldrich, 0.3%, final). For 100-nm liposomes, above concentrations lead to an average of 0.1 transport proteins per liposome. In

case liposomes of different size were used, concentrations were adjusted accordingly to maintain the protein/liposome ratio.

3. Add BioBeads SM2 (BioRad, 40 mg/mL mixture) to remove detergent and gently agitate. Fresh BioBeads are added after the following periods (old beads remain in the solution): 15 min, 15 min, 30 min, overnight, and 60 min. Next, remove BioBeads and store the solution in 100 μL aliquots in liquid nitrogen. One aliquot can be thawed on the experimental day and suffices for 1 day of single-molecule experiments (see later).
4. *Optional*: In order to incorporate additional molecules, such as substrates or nucleotides, in the lumen of the vesicles, mix proteoliposomes with these components prior to the experiment. It should be noted that a concentration of 3.2 μ*M* equates to on average 1 molecule in a 100-nm liposome (see step 2).
5. Subject the solution to four freeze–thaw cycles to homogenize the sample and extrude proteoliposomes at 100 nm (or the relevant size).
6. *Optional*: Excess extraluminal components will be washed away during microscopy experiments (see later), however, an extra washing step (i.e., centrifugation of the proteoliposomes followed by resuspension) can aid this removal process. In case soluble His-tagged protein was used throughout the procedure, excess extraluminal protein can be removed by incubating the solution with Ni-NTA magnetic agarose beads (Qiagen) for 1 h in a reaction tube and extracting them with a magnet.

3. SINGLE-MOLECULE FLUORESCENCE MICROSCOPY

Although chemical and photophysical properties of fluorophores are constantly being improved (van der Velde et al., 2016), they do have a limited rate and number of photons emitted before they permanently bleach into a dark state (Ha & Tinnefeld, 2012). These limitations result in a requirement for efficient and low-background detection of emission light. The first need is realized by high-quality optics and high-sensitivity single-photon detectors. Minimizing the amount of background photons, mainly originating from scattering and impurities, can be done in two ways. In confocal imaging, the detection volume is minimized to volumes on the order of femtoliters (Pawley, 2006), thereby typically allowing only one molecule to be measured. The molecule can be either freely diffusing or immobilized on a surface. A point detector captures all photons originating from the detection volume. An alternative method to reduce background photons, which we also employ here, is to decrease the excitation volume

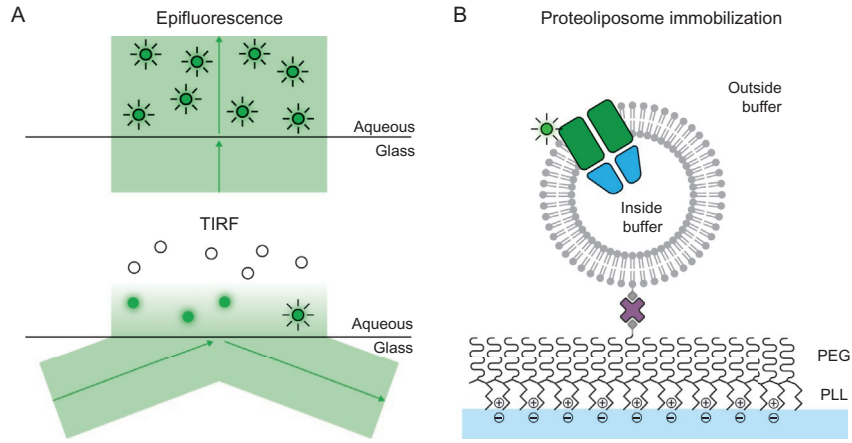

Fig. 3 Microscope setup. (A) Microscopy principles. In epifluorescence (*top*), the entire aqueous solution is excited by the light beam, whereas in TIRF (*bottom*) only a shallow layer (~100–200 nm) on top of the glass surface is excited. (B) Surface immobilization of proteoliposomes. Extensively cleaned glass (negatively charged) is coated with PEG-PLL (positively charged). A small fraction of the PEGs is modified with biotin to allow for immobilization of proteoliposomes containing biotinylated lipids via streptavidin.

by using TIRF microscopy (Axelrod, 2001) (Fig. 3A). As opposed to epifluorescence, where the excitation light beam crosses through the entire sample, TIRF relies on an incident excitation light beam that is totally reflected inside a glass coverslip, thereby creating an evanescent wave of approximately 100–200 nm thick in the medium above the glass. As a result, only fluorophores that are close to the surface will be excited. Here, we use streptavidin to immobilize proteoliposomes containing biotinylated lipids to a glass cover slide coated with poly-L-lysine (PLL) grafted with biotinylated polyethylene glycol (PEG) (see later) (Fig. 3B). Emitted photons are projected on a two-dimensional camera, which enables the recording of multiple fluorophores in parallel. In order to separate fluorescence FRET signals and record two colors simultaneously, we make use of a two-channel simultaneous imaging system that is placed in front of the camera. On top of the glass cover slide used for imaging, a flow cell is constructed that allows for rapid variation of environmental conditions such as pH or substrate concentration, as described in more detail later.

3.1 Glass Functionalization and Flow Cell Construction

A flow cell is constructed based on a functionalized glass cover slide (Fig. 4A). Functionalization of the glass surface is adapted from Tabaei,

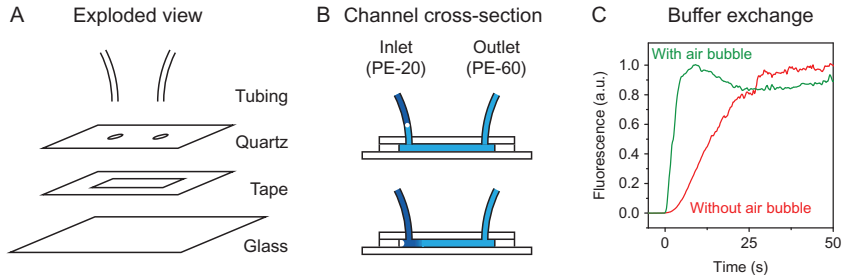

Fig. 4 Flow cell design for rapid buffer exchange. (A) Flow cells were constructed by sandwiching double-sided tape, with a channel (2 cm × 5 mm) excised, between an extensively cleaned glass slip and a reusable quartz plate. (B) Mixing of the buffers is prevented before entering the flow cell by allowing a tiny air bubble, which physically separates the two buffers, in the inlet tube. Upon entering the channel, the air bubble gets trapped, allowing the two buffers to form one continuous phase. (C) The sharp interface only starts to diffuse inside the channel. As a result, at the measurement point, a sharp buffer transition is observed (80% increase within 2 s), as opposed to the case when diffusion already takes place in the inlet tube when no air bubble is present. In this calibration experiment, rhodamine B is used to stain the liquid.

Rabe, Zetterberg, Zhdanov, and Hook (2013). Extensively cleaned glass with a negative surface charge binds to positively charged PLL grafted with polyethylene glycol (PLL-PEG, a fraction of which is biotinylated) to form a biocompatible monolayer that exhibits minimal interaction with proteins and lipids. Cleaned glass surfaces can be stored under vacuum for a few weeks and can later be used to construct a flow cell. The flow cell, which allows for a fast exchange in buffer with a steep gradient (see later) (Fig. 4B and C), can be prepared the day prior to the experiment. Functionalization of the glass surface and attachment of the liposomes happens immediately before performing the single-molecule experiment.

1. Clean microscope cover glass (no. 1.5 precision coverslips, Karl Roth) by sonication in isopropanol for 20 min.
2. Rinse with ultrapure water.
3. Clean microscope cover glass by sonication in acetone for 20 min.
4. Blow-dry with nitrogen gas.
5. Perform oxygen plasma cleaning (Plasma Etch, PE-50) of dried glasses for 10 min to remove remaining organic impurities. Inside the plasma cleaner, the clean side of the glass faces up.

As indicated earlier, cleaned glass slides can be stored in vacuum for some time, before using it to construct a flow cell. All rinsing and incubation steps described later are performed by connecting a syringe to the outlet tube and

creating a light vacuum—the inlet tube resides in a tube with the desired buffer.

6. A channel, 2 cm long and 5 mm wide, is cut out of biocompatible double-sided tape (Grace BioLabs, SecureSeal; 170 μm thick) which is sandwiched between the extensively cleaned thin glass slide and a 1-mm thick quartz plate (Technical Glass) (Fig. 4A). The plate is reusable after soaking the flow cell in acetone to dissolve tape and epoxy and subsequent thorough cleaning of the quartz with acetone. In the quartz plate, two holes are predrilled which tightly fit inlet and outlet tubing of the flow cell. Note that the channel extends beyond the inlet, which allows for fast buffer exchange (described later).
7. Seal the flow cell around the upper quartz plate with generic-brand quick-dry epoxy glue.
8. Insert polyethylene inlet tubing (PE-20, inner and outer diameter 0.4 mm and 1.1 mm, respectively) and outlet tubing (PE-60, inner and outer diameter 0.8 mm and 1.2 mm, respectively) in the holes inside the top quartz plate. Support the tubing and seal the bases of the tubes with epoxy glue and let dry overnight.
9. Incubate the flow cell with 1 *M* KOH for 30 min to remove hydroxyl groups from the glass surface, making it negatively charged.
10. Rinse the channel with copious amounts of ultrapure water and wash with 5 mL PBS buffer.
11. Add a mixture (250 μL should be sufficient) of 1 mg/mL PLL-PEG (PLL(20)-g[3.5]-PEG(2), SuSoS) and 2 μg/mL PLL-PEG-biotin (PLL(20)-g[3.5]-PEG(2)/PEG(3.4)-biotin (20%), SuSoS) and incubate for 30 min.
12. Wash the channel with 5 mL PBS buffer. Purge the channel of any air by pulling a strong vacuum in the syringe connected to the outlet tube; flick the tubing to remove any air bubbles stuck to the inner surface. From this point onward, ensure no unwanted air bubbles enter into the tube/channel.

3.2 Experimental Setup and Image Acquisition

At this point, the flow cell can be mounted on the TIRF microscope. We use an Olympus IX-71 inverted microscope using a 100× high-numerical aperture TIRF objective to visualize immobilized proteoliposomes. The outlet tube of the flow cell is now connected to a programmable syringe pump (NE-1000, New Era Pump Systems, Inc.) that precisely controls

the flow. The inlet tube resides in a reaction tube with the desired buffer. For a rapid response of the pump, no air should be allowed in the outlet tubing and syringe. A 488, 532, and 637 nm laser were installed to excite the dyes. We use an EM-CCD camera (Hamamatsu Photonics) at the highest EM-gain and a frame rate of 5–10 Hz in combination with a two-channel simultaneous imaging system (DV2, Photometrics) (also termed dual view) to record fluorescence simultaneously in multiple colors. The filters in the dual view are optimized for the excitation and emission wavelengths of the dyes. In case of a FRET acquisition, information is needed about the stoichiometry of donor and acceptor dyes. Therefore, FRET acquisitions are preceded and followed by a 5 s period of acceptor only excitation (Kapanidis et al., 2005).

In order to decrease photobleaching and reduce blinking of the dyes (Ha & Tinnefeld, 2012), we use freshly degassed buffer A (by placing it for 30 min in a vacuum desiccator) with the GODCAT oxygen scavenging system (Blanchard, Kim, Gonzalez, Puglisi, & Chu, 2004) (7.5 U/mL glucose oxidase (glucose oxidase from *Aspergillus niger* type VII, Sigma-Aldrich), 450 U/mL catalase (catalase from bovine liver, Sigma-Aldrich), and 0.8% (w/v) glucose monohydrate) and the antiblinking agent Trolox (1 m*M*, prepared as described previously by Cordes, Vogelsang, & Tinnefeld, 2009) (imaging buffer).

1. Incubate the channel with 1.0 mg/mL bovine serum albumin in PBS (buffer C) for 5 min.
2. Incubate with 0.1 mg/mL streptavidin (streptavidin from *Streptomyces avidinii*, Sigma-Aldrich) in buffer C for 5 min.
3. Wash out unbound streptavidin with 5 mL buffer C.
4. Introduce fresh proteoliposomes diluted to 100 μg/mL (1.5 n*M* 100-nm liposomes) in buffer A and incubate for 10 min. The concentration and incubation time can be optimized for good surface coverage—around three spots per 10 μm^2 results a good yield and is not too dense such that single spots cannot be clearly discriminated anymore.
5. Wash out unbound proteoliposomes with 1 mL of buffer A.
6. Prepare for imaging by introducing 1 mL of imaging buffer.
7. Start imaging. During image acquisition, imaging buffer complemented with other components such as substrate or ATP can rapidly be introduced by allowing a small air bubble (~0.2 μL), which will not traverse the flow cell, between the old and new buffer (Fig. 4B and C). This air bubble can be introduced in the inlet tube and moved to a fixed position before starting the acquisition. To do so, remove the inlet tube from the

reaction tube and raise the inlet tube such that a concave meniscus emerges at the end of the tube. Now, put the inlet tube (held steady) into a new reaction tube by moving the reaction tube up. Run the pump for a short time to move the air bubble to the desired position. During acquisition, start the pump to rapidly introduce the new buffer. The exact moment the new buffer arrives at the measurement point can be found with a proper calibration experiment, for example with a rhodamine B solution (Fig. 4C).

4. DATA ANALYSIS

A recording typically contains fluorescence traces of a few hundred spots (Fig. 5A). Before these data can be analyzed further, they have to be processed to correct for artifacts introduced by components in the setup such as lasers, microscope, and camera. The following subsections explain the removal of these artifacts step by step. All algorithms are implemented in in-house written software for ImageJ (Schneider, Rasband, & Eliceiri, 2012). All steps of the algorithms are depicted later, however, an in-depth review of the implementation is beyond the scope of this chapter.

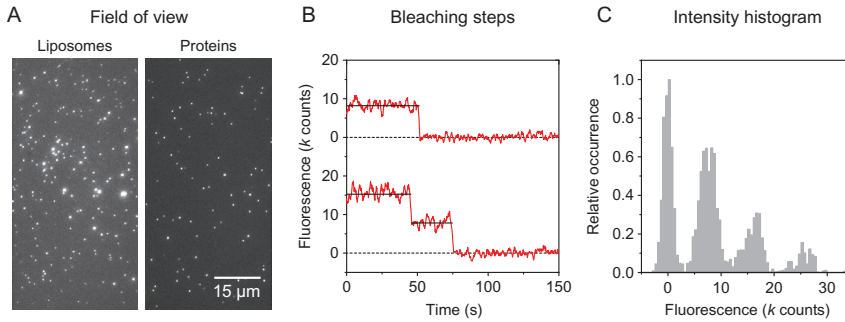

Fig. 5 Typical experimental data. (A) Typical field of view (raw, uncorrected data) with dual view system, allowing for simultaneous acquisition of two colors. Left channel: stained liposomes (DiI). Right channel: soluble proteins in the lumen of these liposomes (BtuF, labeled with Alexa Fluor 647). (B) Bleaching steps of BtuF originating from two spots in (A). Steps are identified manually here and intermediate intensity levels are fitted (*solid black line*). (C) Creating a histogram based on data from a bleaching experiment (11 traces) reveals that single fluorophores have an intensity between 5000 and 12,000 counts, which corresponds to a step size as observed in (B).

4.1 Subtraction of Electronic Offset

The EM-CCD camera introduces a constant hardware electronic offset to all pixels such that noise will never generate negative values (the computer files are stored in positive integer values only). The value of the offset can readily be obtained by closing the shutter in front of the camera and minimizing the exposure time. The average value of a single frame can then be used as offset to subtract from the movie, which is now stored in a format that allows signed values.

4.2 Laser Profile Correction

The Gaussian profile of the laser beam is clearly visible in the emission intensities of the spots in the field of view. A map of intensity values, normalized to one and with the same dimensions as the recording, is used to divide each frame of the movie. This map can be created by a long exposure image, while the field of view is continuously moved in both lateral directions. The image can be smoothened by a 32-pixel radius Gaussian filter. The resulting map, of course, has to be corrected for electronic offset as well.

4.3 Dual View Alignment

The two-channel simultaneous imaging system splits the image on the camera in two halves, each for light at a different wavelength. Owing to chromatic aberrations and imperfections in the optics of the system, coordinates in one half are not merely a lateral translation of coordinates in the other half. A second-order two-dimensional polynomial is used to map points from one halve to the other:

$$\Delta x = a_0 + a_1 x + a_2 y + a_3 x^2 + a_4 xy + a_5 y^2,$$
$$\Delta y = b_0 + b_1 x + b_2 y + b_3 x^2 + b_4 xy + b_5 y^2.$$

Here, Δx and Δy are the lateral displacements of the corresponding coordinates (x, y) and (x', y') in each halve:

$$x' = x + \Delta x,\ y' = y + \Delta y.$$

The parameters a_i and b_i of the polynomial are determined by using a dataset that has signals originating from the same point simultaneously in both channels. Peak positions are identified independently in both channels (although most signals should originate from the same spot, not all points necessarily have to form pairs) using MaximumFinder in ImageJ. Subsequently, two binary-valued images (one for each channel) are created with

single-pixel peaks on a black background and registered using a combination of mixture of Gaussians (Jian & Vemuri, 2005) and two-dimensional fitting using the Levenberg–Marquardt algorithm. In a next step, overlapping fluorescent points can easily be identified in both channels, which is needed in, e.g., FRET measurements or colocalization experiments with stained liposomes and fluorescently labeled proteins.

4.4 Drift Correction

Long-duration acquisitions of several minutes can be affected by stage drift. Subsequent images in the recording can therefore be registered with the first image by applying FFT-based techniques for subpixel translational image registration (Guizar-Sicairos, Thurman, & Fienup, 2008; Reddy & Chatterji, 1996).

4.5 Data Analysis

Peaks are detected by MaximumFinder in ImageJ. Fluorescence traces, corrected for all artifacts as described earlier, are constructed by plotting the integrated intensity in a 7-pixel diameter circle around a peak. Integrated background intensity, extracted from a nearby area devoid of peaks and normalized to a 7-pixel diameter circle, is subtracted after a 25-frame temporal median filter is applied. Shot noise and electronic noise are removed from the resulting traces by applying a 5-frame temporal mean filter. Traces are finally corrected for cross-talk between the donor and acceptor channel: bleeding of donor signal into the acceptor channel and vice versa. These values can be derived from the spectral properties of the filters and fluorophores, and it can easily be verified experimentally by having only donor or only acceptor molecules present.

The stoichiometry of fluorescent labels, both in single and dual-color images, is important for further analysis. For example, in FRET measurements, it is important to have one donor and one acceptor. Furthermore, the number of labeled proteins in the membrane or lumen of liposomes can also contain valuable information. The number of dye molecules can be obtained by determination of discrete bleaching steps—the hallmark of single-molecule traces (Fig. 5B). This procedure requires the detection of change points in the fluorescence trace, which we will describe later. If these data are not available, or bleaching is unwanted, the intensity of a single fluorophore needs to be determined. After creating a histogram of all fluorescence intensity values, it is possible to assign a number of fluorophores to

the amount of fluorescence (Fig. 5C). This information can be used later in experiments with identical fluorescent dyes and laser power to assess the number of dyes or proteins.

Change points in fluorescence transients are indicative for conformational changes of the labeled protein or bleaching as described earlier. They can be detected in several ways. The most common and straightforward way is by thresholding. If prior knowledge exists about the different fluorescence states, for example by examining the histogram of all intensity values of dynamic traces, each time point can be assigned to a distinct fluorescence intensity level. Without prior information, a jump can be detected by identifying for example a change, between two adjacent time points, which magnitude exceeds three times (this value is adjustable) the standard deviation of the signal before the change. Often, this simple and fast algorithm does not perform well, as slow or small changes will not be detected. A more sophisticated technique that can be applied is a method that uses a generalized likelihood ratio test to find change points (Watkins & Yang, 2005). For FRET time series, if the protein complex transitions between stable conformations, modeling can be done by a hidden Markov model (HMM). Several software packages have been developed that adapt HMM to analyze FRET traces (Bronson, Fei, Hofman, Gonzalez, & Wiggins, 2009; McKinney, Joo, & Ha, 2006). Further analysis of the data, which depends on the system being studied, is highly specific and is therefore beyond the scope of this chapter.

ACKNOWLEDGMENTS

D.J.S. would like to acknowledge funding from the Netherlands Organization for Scientific Research (NWO) (Vici grant 865.11.001) and the European Research Council (ERC) (ERC Starting Grant 282083). A.v.O. acknowledges support by the European Research Council (ERC) (ERC Starting Grant 281098), the Netherlands Organization for Scientific Research (NWO) (Vici grant 680.47.607), and the Australian Research Council (Laureate Fellowship FL140100027).

REFERENCES

Akyuz, N., Altman, R. B., Blanchard, S. C., & Boudker, O. (2013). Transport dynamics in a glutamate transporter homologue. *Nature*, *502*(7469), 114–118. http://dx.doi.org/10.1038/nature12265.

Axelrod, D. (2001). Total internal reflection fluorescence microscopy in cell biology. *Traffic*, *2*(11), 764–774.

Blanchard, S. C., Kim, H. D., Gonzalez, R. L., Jr., Puglisi, J. D., & Chu, S. (2004). tRNA dynamics on the ribosome during translation. *Proceedings of the National Academy of Sciences of the United States of America*, *101*(35), 12893–12898. http://dx.doi.org/10.1073/pnas.0403884101.

Bronson, J. E., Fei, J., Hofman, J. M., Gonzalez, R. L., Jr., & Wiggins, C. H. (2009). Learning rates and states from biophysical time series: A Bayesian approach to model selection and single-molecule FRET data. *Biophysical Journal*, *97*(12), 3196–3205. http://dx.doi.org/10.1016/j.bpj.2009.09.031.

Brooks Shera, E., Seitzinger, N. K., Davis, L. M., Keller, R. A., & Soper, S. A. (1990). Detection of single fluorescent molecules. *Chemical Physics Letters*, *174*(6), 553–557. http://dx.doi.org/10.1016/0009-2614(90)85485-U.

Cordes, T., Vogelsang, J., & Tinnefeld, P. (2009). On the mechanism of Trolox as antiblinking and antibleaching reagent. *Journal of the American Chemical Society*, *131*(14), 5018–5019. http://dx.doi.org/10.1021/ja809117z.

Dickson, R. M., Cubitt, A. B., Tsien, R. Y., & Moerner, W. E. (1997). On/off blinking and switching behaviour of single molecules of green fluorescent protein. *Nature*, *388*(6640), 355–358. http://dx.doi.org/10.1038/41048.

Dorwart, M. R., Wray, R., Brautigam, C. A., Jiang, Y., & Blount, P. (2010). *S. aureus* MscL is a pentamer in vivo but of variable stoichiometries in vitro: Implications for detergent-solubilized membrane proteins. *PLoS Biology*, *8*(12), e1000555. http://dx.doi.org/10.1371/journal.pbio.1000555.

Drew, D., & Boudker, O. (2016). Shared molecular mechanisms of membrane transporters. *Annual Review of Biochemistry*, *85*, 543–572. http://dx.doi.org/10.1146/annurev-biochem-060815-014520.

Erkens, G. B., Hanelt, I., Goudsmits, J. M., Slotboom, D. J., & van Oijen, A. M. (2013). Unsynchronised subunit motion in single trimeric sodium-coupled aspartate transporters. *Nature*, *502*(7469), 119–123. http://dx.doi.org/10.1038/nature12538.

Geertsma, E. R., Nik Mahmood, N. A., Schuurman-Wolters, G. K., & Poolman, B. (2008). Membrane reconstitution of ABC transporters and assays of translocator function. *Nature Protocols*, *3*(2), 256–266. http://dx.doi.org/10.1038/nprot.2007.519.

Goudsmits, J. M. H., Slotboom, D. J., & van Oijen, A. M. (2017) Single-molecule visualization of the vitamin B12 transport mechanism of the ABC importer BtuCD-F.

Groeneveld, M., & Slotboom, D. J. (2010). Na(+): Aspartate coupling stoichiometry in the glutamate transporter homologue Glt(Ph). *Biochemistry*, *49*(17), 3511–3513. http://dx.doi.org/10.1021/bi100430s.

Guizar-Sicairos, M., Thurman, S. T., & Fienup, J. R. (2008). Efficient subpixel image registration algorithms. *Optics Letters*, *33*(2), 156–158.

Gust, A., Zander, A., Gietl, A., Holzmeister, P., Schulz, S., Lalkens, B., et al. (2014). A starting point for fluorescence-based single-molecule measurements in biomolecular research. *Molecules*, *19*(10), 15824–15865. http://dx.doi.org/10.3390/molecules191015824.

Ha, T., Enderle, T., Ogletree, D. F., Chemla, D. S., Selvin, P. R., & Weiss, S. (1996). Probing the interaction between two single molecules: Fluorescence resonance energy transfer between a single donor and a single acceptor. *Proceedings of the National Academy of Sciences of the United States of America*, *93*(13), 6264–6268.

Ha, T., & Tinnefeld, P. (2012). Photophysics of fluorescent probes for single-molecule biophysics and super-resolution imaging. *Annual Review of Physical Chemistry*, *63*, 595–617. http://dx.doi.org/10.1146/annurev-physchem-032210-103340.

Helenius, A., & Simons, K. (1975). Solubilization of membranes by detergents. *Biochimica et Biophysica Acta*, *415*(1), 29–79.

Jian, B., & Vemuri, B. C. (2005). A robust algorithm for point set registration using mixture of Gaussians. *Proceedings/IEEE International Conference on Computer Vision*, *2*, 1246–1251. http://dx.doi.org/10.1109/ICCV.2005.17.

Kapanidis, A. N., Laurence, T. A., Lee, N. K., Margeat, E., Kong, X., & Weiss, S. (2005). Alternating-laser excitation of single molecules. *Accounts of Chemical Research*, *38*(7), 523–533. http://dx.doi.org/10.1021/ar0401348.

Krogh, A., Larsson, B., von Heijne, G., & Sonnhammer, E. L. (2001). Predicting transmembrane protein topology with a hidden Markov model: Application to complete genomes. *Journal of Molecular Biology*, *305*(3), 567–580. http://dx.doi.org/10.1006/jmbi.2000.4315.

Lakowicz, J. R. (2006). *Principles of fluorescence spectroscopy* (3rd ed.). New York: Springer.

Lee, A. G. (2003). Lipid–protein interactions in biological membranes: A structural perspective. *Biochimica et Biophysica Acta*, *1612*(1), 1–40.

Lee, A. G. (2004). How lipids affect the activities of integral membrane proteins. *Biochimica et Biophysica Acta*, *1666*(1–2), 62–87. http://dx.doi.org/10.1016/j.bbamem.2004.05.012.

Lewinson, O., Lee, A. T., Locher, K. P., & Rees, D. C. (2010). A distinct mechanism for the ABC transporter BtuCD-BtuF revealed by the dynamics of complex formation. *Nature Structural & Molecular Biology*, *17*(3), 332–338. http://dx.doi.org/10.1038/nsmb.1770.

Lu, H. P., Xun, L., & Xie, X. S. (1998). Single-molecule enzymatic dynamics. *Science*, *282*(5395), 1877–1882.

Marsh, D. (2008). Protein modulation of lipids, and vice-versa, in membranes. *Biochimica et Biophysica Acta*, *1778*(7–8), 1545–1575. http://dx.doi.org/10.1016/j.bbamem.2008.01.015.

McKinney, S. A., Joo, C., & Ha, T. (2006). Analysis of single-molecule FRET trajectories using hidden Markov modeling. *Biophysical Journal*, *91*(5), 1941–1951. http://dx.doi.org/10.1529/biophysj.106.082487.

Mi, L. Z., Grey, M. J., Nishida, N., Walz, T., Lu, C., & Springer, T. A. (2008). Functional and structural stability of the epidermal growth factor receptor in detergent micelles and phospholipid nanodiscs. *Biochemistry*, *47*(39), 10314–10323. http://dx.doi.org/10.1021/bi801006s.

Missner, A., & Pohl, P. (2009). 110 years of the Meyer–Overton rule: Predicting membrane permeability of gases and other small compounds. *ChemPhysChem*, *10*(9–10), 1405–1414. http://dx.doi.org/10.1002/cphc.200900270.

Neher, E., & Sakmann, B. (1976). Single-channel currents recorded from membrane of denervated frog muscle fibres. *Nature*, *260*(5554), 799–802.

Pawley, J. B. (2006). *Handbook of biological confocal microscopy* (3rd ed.). New York: Springer.

Phillips, R., Ursell, T., Wiggins, P., & Sens, P. (2009). Emerging roles for lipids in shaping membrane–protein function. *Nature*, *459*(7245), 379–385. http://dx.doi.org/10.1038/nature08147.

Reddy, B. S., & Chatterji, B. N. (1996). An FFT-based technique for translation, rotation, and scale-invariant image registration. *IEEE Transactions on Image Processing*, *5*(8), 1266–1271. http://dx.doi.org/10.1109/83.506761.

Ren, Q., & Paulsen, I. T. (2005). Comparative analyses of fundamental differences in membrane transport capabilities in prokaryotes and eukaryotes. *PLoS Computational Biology*, *1*(3), e27. http://dx.doi.org/10.1371/journal.pcbi.0010027.

Rigaud, J. L., & Levy, D. (2003). Reconstitution of membrane proteins into liposomes. *Methods in Enzymology*, *372*, 65–86. http://dx.doi.org/10.1016/S0076-6879(03)72004-7.

Ritchie, T. K., Grinkova, Y. V., Bayburt, T. H., Denisov, I. G., Zolnerciks, J. K., Atkins, W. M., et al. (2009). Chapter 11—Reconstitution of membrane proteins in phospholipid bilayer nanodiscs. *Methods in Enzymology*, *464*, 211–231. http://dx.doi.org/10.1016/S0076-6879(09)64011-8.

Ruan, Y., Miyagi, A., Wang, X., Chami, M., Boudker, O., & Scheuring, S. (2017). Direct visualization of glutamate transporter elevator mechanism by high-speed AFM. *Proceedings of the National Academy of Sciences of the United States of America*, *114*(7), 1584–1588. http://dx.doi.org/10.1073/pnas.1616413114.

Saier, M. H., Jr., Reddy, V. S., Tamang, D. G., & Vastermark, A. (2014). The transporter classification database. *Nucleic Acids Research*, *42*(Database issue), D251–D258. http://dx.doi.org/10.1093/nar/gkt1097.

Sako, Y., Minoghchi, S., & Yanagida, T. (2000). Single-molecule imaging of EGFR signalling on the surface of living cells. *Nature Cell Biology*, *2*(3), 168–172. http://dx.doi.org/10.1038/35004044.

Schmidt, T., Schuetz, G. J., Baumgartner, W., Gruber, H. J., & Schindler, H. (1995). Characterization of photophysics and mobility of single molecules in a fluid lipid membrane. *The Journal of Physical Chemistry*, *99*(49), 17662–17668. http://dx.doi.org/10.1021/j100049a030.

Schneider, C. A., Rasband, W. S., & Eliceiri, K. W. (2012). NIH image to ImageJ: 25 years of image analysis. *Nature Methods*, *9*(7), 671–675.

Seddon, A. M., Curnow, P., & Booth, P. J. (2004). Membrane proteins, lipids and detergents: Not just a soap opera. *Biochimica et Biophysica Acta*, *1666*(1–2), 105–117. http://dx.doi.org/10.1016/j.bbamem.2004.04.011.

Tabaei, S. R., Rabe, M., Zetterberg, H., Zhdanov, V. P., & Hook, F. (2013). Single lipid vesicle assay for characterizing single-enzyme kinetics of phospholipid hydrolysis in a complex biological fluid. *Journal of the American Chemical Society*, *135*(38), 14151–14158. http://dx.doi.org/10.1021/ja4046313.

van der Velde, J. H., Oelerich, J., Huang, J., Smit, J. H., Aminian Jazi, A., Galiani, S., et al. (2016). A simple and versatile design concept for fluorophore derivatives with intramolecular photostabilization. *Nature Communications*, 7, 10144. http://dx.doi.org/10.1038/ncomms10144.

Watkins, L. P., & Yang, H. (2005). Detection of intensity change points in time-resolved single-molecule measurements. *The Journal of Physical Chemistry. B*, *109*(1), 617–628. http://dx.doi.org/10.1021/jp0467548.

Weiss, S. (1999). Fluorescence spectroscopy of single biomolecules. *Science*, *283*(5408), 1676–1683.

Whited, A. M., & Park, P. S. (2014). Atomic force microscopy: A multifaceted tool to study membrane proteins and their interactions with ligands. *Biochimica et Biophysica Acta*, *1838*(1 Pt. A), 56–68. http://dx.doi.org/10.1016/j.bbamem.2013.04.011.

Zhao, Y., Terry, D., Shi, L., Weinstein, H., Blanchard, S. C., & Javitch, J. A. (2010). Single-molecule dynamics of gating in a neurotransmitter transporter homologue. *Nature*, *465*(7295), 188–193. http://dx.doi.org/10.1038/nature09057.